Title

NEUTRON DOSIMETRY IN AND AROUND HUMAN PHANTOMS BY USE OF NUCLEAR TRACK EMULSION

Permalink

Authors

Akagi, Hiroaki
Lehman, Richard L.

Publication Date

1961-11-30

University of California

Ernest O. Lawrence Radiation Laboratory

Berkeley, California

DISCLAIMER

UCRL-9967

UNIVERSITY OF CALIFORNIA

Lawrence Radiation Laboratory
Berkeley, California

Contract No. W-7405-eng-48

NEUTRON DOSIMETRY IN AND AROUND HUMAN PHANTOMS BY USE OF NUCLEAR TRACK EMULSION

Hiroaki Akagi and Richard L. Lehman

November 30, 1961

NEUTRON DOSIMETRY IN AND AROUND HUMAN PHANTOMS BY USE OF NUCLEAR TRACK EMULSION

Hiroaki Akagi and Richard L. Lehman

Lawrence Radiation Laboratory
University of California
Berkeley, California

November 30, 1961

Abstract

The power of nuclear track research emulsion as a fast neutron dosimeter is examined in the exposure of a human phantom to PuBe neutrons. Semiautomatic track scanning and high-speed data analysis obviate the major disadvantages of this dosimeter, and allow the following basic information to be obtained without a serious cost in time: the relative proton recoil energy spectrum, the absolute differential proton track density spectrum, and the average proton recoil energy at various locations in the phantom. From this are calculated the total absorbed local tissue dose due is proton recoils, the local thermal neutron intensity, and that portion of the tissue dose due to thermal N(n,p)C tracks.

NEUTRON DOSIMETRY IN AND AROUND HUMAN PHANTOMS BY USE OF NUCLEAR TRACK EMULSION

Studies with Plutonium-Beryllium Neutrons

Hiroaki Akagi and Richard L. Lehman

Lawrence Radiation Laboratory
University of California
Berkeley, California

November 30, 1961

I. INTRODUCTION

Nuclear track emulsion has been widely used for detection and measurement since the beginning of neutron research. However, health physicists have not until now shown much interest in this tool, which is probably the best single neutron dosimeter. The reason for this lack of interest is simple: track scanning and analysis require a great deal of time. Now semiautomatic scanning of emulsions and data analysis by electronic computer have partly overcome this difficulty. But the question arises--"How good is this tool for analyzing tissue dose from neutron exposure?"

In an attempt to answer this question, nuclear track emulsion was exposed in and around human phantoms to various kinds of neutrons. In this report we present data obtained from exposure to plutonium-beryllium neutrons. These data include the proton recoil energy distribution, absolute differential track density, and emulsion dose at various depths in the phantom. From this the tissue dose is calculated.

II. EXPERIMENTAL METHOD

The nuclear emulsions (Ilford L.4 and Kodak NTA) were exposed by the PuBe source, in a wooden room, 4 × 5m × 3m high, in and around the human phantom, details of which are shown in Figs. 1 and 2 Tracks in the developed emulsions were scanned and analyzed.

Neutron source

LRL source PuBe #593 was used. It is a cylinder, 1.30 in. o.d. $\times$ 3.69 in. high, containing 80 g of plutonium. The total emission rate was 5.89×10^6 n/sec.

Nuclear emulsions

Ilford L.4 600-micron emulsions were cut into four pieces (27 $\times$ 2.5 mm or 1 $\times$ 3/4 in.) from an original piece (1 $\times$ 3 in.), and each was wrapped with black paper and black tape. Each emulsion was sealed in a 20-mil polyvinyl packet with Kodak NTA type film. Each packet was so oriented that the emulsions were exposed normal to the source, which was 50 cm from the center of the phantom.

Phantom

The human phantom was a right elliptical cyclinder, 20 $\times$ 36 cm by 60 cm high made of 0.65-cm polyethylene (Figs. 1 and 2) and filled with tissue-equivalent fluid.* It stood on a support 76 cm above the floor. Six polyvinyl packets of films (C-1 through C-5, and C-9) were kept during the exposure on the mid-horizontal plane of the phantom with a thin plastic plate. Figure 2 shows the locations of these packets.

---

*Tissue-equivalent fluid:

H_2O,	75 lb;
urea,	9.46 lb;
sucrose,	24.7 lb;
cresol,	1.05 lb.

Developing and fixing

After the exposure of 87 hours and 20 minutes, the L.4 films were opened in a darkroom and were measured for thickness and lateral extent. They were then developed and fixed by a modified cold-cycle process* in which the solutions were kept at 5°C. To reduce thickness shrinkage, the processed emulsions were soaked in a concentrated solution of wood rosin in ethanol (35 g per 100 ml) for 24 hr. Emulsion history charts (Fig. 3) were kept for each film. The thickness and lateral extent of the processed films were remeasured and the shrinkage factors f_1 and f_2 were calculated for each emulsion. Prior to scanning, films were mounted on 1 × 3 in. microslides with clear epoxy cement.

The NTA films were developed according to the usual method.

Scanning

The Ilford films were scanned by use of the three-axis digitized microscope and apparatus in Figs. 4 and 5. The date, the relative humidity at the time of scanning, the emulsion number, and the end-point

---

*A modified cold-cycle process:

45 min	water (presoak)
90 min	developer: Na_2SO_3, 3.6g.; $Na_2S_2O_5$, 0.5g.; 10% KBr solution, 4.4 ml; Amidol, 1.6g.; H_2O, 500 ml
45 min	stop bath: HAc, 1 ml; H_2O, 500 ml
18 hr	fix: $Na_2S_2O_3$, 150 g.; $Na_2S_2O_5$, 11.2g.; H_2O, 500 ml
4 hr	water (dilution and washing)
3 hr	EtOH (to dry): gradual dilution to 100% EtOH
24 hr	rosin (soak)
2 hr	air (to dry between silk)

coordinates of two tracks were recorded on each punched card. The microscope was fitted with a 65X oil-immersion objective and 10X wide-field eyepieces. It required 6 to 7 hr to scan 1200 tracks.

To obtain an unbiased sample of the tracks in an emulsion, we took a "random walk" through the emulsion, seeking out the track ending nearest to the end point of the previous track. Only tracks which had both end points within the emulsion were recorded.

Analysis of tracks in nuclear emulsions

The punched cards were analyzed by an IBM-650 Computer with a special computer program called "RECOIL I". This program is designed to calculate the proton recoil energy spectrum in nuclear emulsion exposed to neutrons. The following conditions apply to "RECOIL I".

a. The emulsion must be of 625 microns nominal initial thickness.

b. The emulsion must be of "standard" composition, i. e., density ≈ 3.8 at 50% relative humidity and 20°C.

c. The input tracks scanned must be a random sample of the tracks present in the emulsion.

There is no condition on the isotropy or angle of exposure. The input to RECOIL I consists of rectangular coordinates (x_1 y_1 z_1, x_2 y_2 z_2) for the beginning and end points of a track measured in the emulsion. For each track a correct length in microns is computed,

$$\ell = (f_1^{\,2}\,\Delta x^2 + f_1^{\,2}\,\Delta y^2 + f_2^{\,2}\,\Delta z^2)^{1/2}$$

where ℓ is the length of the track, f_1 is the correction factor for the lateral (x, y) shrinkage, and f_2 is a correction containing the thickness (z) shrinkage factor. The Δx i. e., $(x_1 - x_2)$ and Δy i. e., $(y_1 - y_2)$ are in units of microns, but Δz is in units of 0.60 micron. Therefore the correction f_2 is the product of 0.60 $\times$ the z shrinkage factor. The program compares the computed length with a range-energy table for protons in nuclear emulsion[1], and the track is sorted into one of 85 energy intervals. Several hundred tracks thus generate the points of a raw proton-recoil energy spectrum.

RECOIL I corrects the raw proton spectrum by a function based on geometry. This function gives the probability that a track of a given length which originates in the emulsion will end in the emulsion. Using 625 μ for the emulsion thickness at exposure, and assuming an infinite lateral extent for the emulsion (although the actual size is as small as a 2.0-cm square), we find this function is

$$P = \frac{625 - 0.5\ell}{625} \quad \text{for } \ell < 625 \text{ microns,}$$

and

$$P = \frac{322}{\ell} \quad \text{for } \ell > 625 \text{ microns.}$$

Each point on the spectrum is also corrected by its energy interval. RECOIL I thus computes 85 proton-recoil spectrum points $\frac{\Delta N}{P\Delta E}$ and the standard deviation $\frac{\sqrt{\Delta N}}{P\Delta E}$ for each point, where ΔN is the number of tracks in energy interval ΔE and P is the geometry correction. In addition, the track density in the L.4 films was independently measured by counting the number of tracks (in depth) in from 6 to 28 fields of view. The volume per field was 3.34×10^{-5} cm^3.

The number of tracks in depth per field of view for NTA was measured by the standard method. The field was 0.00060 cm^2 when 450$\times$ magnification was used.

III. RESULTS

The proton-recoil spectra in and around the human phantom, as computed from tracks scanned in Ilford L.4 emulsions C-1 through C-5 and C-9, are given in Table 1. The values shown are $\frac{\Delta N}{P\Delta E}$ normalized to give $\Sigma \frac{\Delta N}{P\Delta E} = 1.000$. The normalization allows direct comparison of the spectra, channel by channel, and these values are plotted in Figs. 6 through 11.

The same data are plotted in Fig. 12 to show the absolute track density. In this figure the points are first normalized to give $\Sigma \frac{\Delta N}{P} = 1.00$ (i.e., the area under the $\frac{\Delta N}{P\Delta E}$ vs E curve is 1.00 in each case.) Then the points are fortified by the absolute track density (Fig. 13) in the emulsion which gave rise to them, and are corrected by the inverse square to a true distance of 50 cm from the neutron source.

The Kodak NTA response to the neutron irradiation at various depths in the phantom is presented in Fig. 14.

Average energy and absorbed dose of proton recoils in the emulsions at various depths in the phantom were found as follows. To obtain the average energy of the proton recoils (Fig. 15) we calculated

$$\Sigma \frac{\Delta N}{P\Delta E} \cdot E \cdot \Delta E / \Sigma \frac{\Delta N}{P\Delta E} ; \Delta E$$ for the Ilford films C-1 to C-5, and C-9. The energy absorbed in the emulsion from proton recoils (Fig. 16) at various phantom depths is the product of the measured absolute track density and the average energy per track.

IV. DISCUSSION

The estimate of biological damage from ionizing radiation is usually based on the knowledge of the amount of energy imparted to the tissue and by what means, and on the energy distribution of the particles involved. The major part of the dose delivered by fast neutrons to tissue arises from hydrogen nuclei recoiling from elastic collision with the neutrons. In order to understand the biological effects of neutrons in humans it is necessary to know the detailed proton-recoil energy distribution at various depths within the body. Therefore, a suitable tissue neutron dosimeter is one that does not influence the local neutron distribution. Further, it must record exactly the recoil events in space, and it must be of small size. It is also desirable that the dosimeter be continuously sensitive, that it have a low gamma sensitivity, that many simultaneous measurements can be made, that the time between exposure and analysis be convenient, and that a permanent record be made. It is clear that nuclear track emulsion is superior to other dosimeters in these respects.

Table 2 gives the basic data concerning the effect of the presence track emulsion on the local neutron distribution in tissue. The table reveals that for fast neutrons the total macroscopic cross sections of tissue and emulsion are nearly the same. Therefore the presence of emulsion is not expected to perturb the local fast-neutron spectra at various depths in tissue.

When fast neutrons impinge on the human body, large numbers of thermal neutrons are produced as the fast neutrons lose energy through multiple collisions. This is why the effect of a dosimeter on the local thermal-neutron density must also be considered. The ratio of the macroscopic absorption cross section for thermal neutrons in emulsion and in tissue is about 30/1. However, this does not appear to be important when the mean-square diffusion distance (as the crow flies) of thermal neutrons is compared to the emulsion thickness. This "distance" is about 16 cm^2 in tissue and 1 cm^2 in emulsion; the emulsion thickness is 0.060 cm. This means that the average net distance that a neutron travels from the time when it is produced until the time when it is captured is about 1 cm in emulsion and 4 cm in tissue. Therefore the thermal neutron density in the emulsion is not expected to differ from that in nearby tissue.

1. Interpretation of the track density distributions.

The major feature of these track spectra, as revealed in Fig. 13, is that from about 0.8 Mev to higher energies the track density decreases exponentially. In this region the track density follows the relation $\frac{dN}{dE} \propto e^{-0.836\,E}$ for all depths. This track-density distribution is exactly what one theoretically expects for a PuBe neutron exposure of emulsion in air*. The finding that the same distribution obtains at various depth in emulsion indicates that the major features of the neutron spectrum are present even deep in the phantom. Proton recoil tracks from the thermal $N^{14}(n,p)C^{14}$ reaction, and from secondary neutron collisions with hydrogen nuclei, are superimposed on the basic distributions. The n, p tracks are monoenergetic at 0.60 Mev and are quite prominent in the track spectra of emulsions C-2,

*The expected track-density distribution was calculated from unpublished data on the PuBe neutron spectrum obtained by Lehman.

C-3, and C-4. The secondary-collision tracks are largely below 1.5 Mev and are evident in the track spectra C-1 to C-4. The track density spectrum of C-5 shows the $e^{-0.836 E}$ pattern with a relatively small thermal-neutron N(n, p)C peak and virtually no secondary-neutron collision peak.

Below 0.5 Mev, the efficiency of nuclear emulsion drops rapidly, giving the erroneous picture that the number of tracks falls. The track densities are expected to be about the same from 0.5 to 0 Mev as they are at 0.5 Mev.

2. Separation of the thermal $N^{14}(n, p) C^{14}$ track component, and estimation of the thermal neutron intensities.

For determining proton-recoil emulsion dose there is no need to separate the component due to n, p tracks, but it is important that this be done for calculating tissue dose.

The thermal n, p track contribution was estimated by subtracting the percent of the tracks in the 0.5- to -1.0-Mev interval of the C-9 distribution (in which we assume there are no n, p tracks) from the percent in the same region in emulsions C-1 through C-5:

percent of thermal-neutron n, p tracks =

$$A_i - (1 - A_i)\, k, \tag{1}$$

where A_i is the percent of tracks in the 0.5- to -1.0-Mev region for the emulsion under consideration and k is $A/(1-A)$ for emulsion C-9. Table 3 gives the result.

3. Interpretation of total L.4 track density and total NTA response vs depth in phantom.

The major feature of the plots in Figs. 14 and 15 is the exponential attenuation of neutrons with depth with an attenuation half thickness of

6.5 cm. This attenuation is for all fast neutrons present in the phantom that are detectable by nuclear track emulsion. Superimposed on this basic response is the response due to thermal-neutron N(n, p)C tracks. It is this thermal-neutron response that distorts the basic 6.5 cm attenuation in the L.4 plot. The following brief explanation is an attempt to clarify this.

The NTA response to neutron exposure, in tracks/field, may be represented by the equation

$$\text{NTA response} = an^{th} + bn^{f}. \qquad (2)$$

Similarly, the L.4 response, in tracks/cm^3, may be represented by

$$\text{L.4 response} = cn^{th} + dn^{f}. \qquad (3)$$

In these equations, the coefficients a and b have the dimensions of tracks/field per unit thermal neutron (n^{th}) or fast neutron (n^{f}) per cm^2. The coefficients c and d have the dimensions tracks/cm^3 per unit thermal- or fast-neutron exposure. The difference in shape between Figs. 14 and 15 arises because $c/d \approx 3\ a/b$ for PuBe neutrons, that is, the relative response of L.4 to thermal neutrons is roughly three times that of NTA. The reason that these ratios differ is that the NTA response includes ~~tracks which originate~~ in adjacent hydrogenous radiator material,[2] whereas the L.4 response does not. (Only tracks that begin and end within the L.4 emulsion are scanned.)

4. Calculation of tissue dose vs. depth in the phantom

Table 4 gives the absorbed proton recoil energy per cm^3 in L.4 and in tissue-equivalent liquid at various depths in the phantom. To obtain the tissue thermal-neutron n, p track dose, the L.4 dose is multiplied by 0.406, the ratio of the nitrogen atomic density in tissue to that in

L. 4 emulsion. (The result is plotted in Fig. 16 where the n, p tissue dose calculated here is compared with the relative thermal neutron density measured by indium foil activation.) To obtain the fast neutron proton track dose, the L. 4 dose is multiplied by 1.86, the ratio of the atomic density of hydrogen in tissue to that in L. 4 emulsion. In no case does the tissue thermal n, p track dose exceed 3% of the total tissue proton dose.

From the calculation of the track distribution in emulsion exposed in air to PuBe neutrons, mentioned in Section 1, 24% of the proton tracks are expected to have energy between 0 and 0.50 Mev. Nuclear emulsion does not detect these tracks. However, since they contribute only about 4% of the absorbed tissue dose, the data in this report are not corrected for them.

5. Comparison of phantom proton dose with a predicted dose

In Handbook 63[3] the tissue proton dose is calculated by assuming exposure of an infinite 30-cm-thick tissue-equivalent slab to monoenergetic neutrons of various energies. Table 5 compares the data for 2.5- and 5.0-Mev neutrons with our phantom data for PuBe neutrons. Two things are evident--the first is that at all depths our values are roughly 1/2 the 5.0-Mev values in Handbook 63. The second is that the proton dose attenuation with depth shows a half-thickness value of 10 cm for the phantom exposed to PuBe neutrons (Fig. 17), but 5.5 cm and 8.5 cm for the slab exposed to 2.5- and 5.0-Mev neutrons.

A large part of the discrepancy between our values and the values of Handbook 63 for the absolute magnitude of the proton dose lies in the fact that Handbook 63 uses a value of 2.50 Mev for the average first-collision energy transfer between a 5.0-Mev neutron and a hydrogen nucleus. We found that the average energy of the recoil tracks in the C-1 to C-5 spectra (excluding thermal n, p tracks) varied between 1.42 and 1.76 Mev at the different depths, compared with 1.61 Mev in emulsion C-9, which was exposed in air. The values at the 0-cm and 5-cm depths are much lower than 1.51 Mev; this is evidence for a significant track contribution from second-collision neutrons.

At 10 cm depth the average recoil proton energy is 1.60 Mev--almost exactly the same as that in emulsion exposed in free air. This may be the result of the second-collision portion compensating for the low-energy neutron component which is selectively filtered out by 10 cm of tissue. The average proton track energy at the back surface of the phantom (C-5) is 1.76 Mev--a surprisingly low value, since very few tracks here arise from secondary-neutron collision. This reveals that although there is some hardening of primary neutron spectrum, many low-energy neutrons are present.

V. SUMMARY

The power of nuclear track emulsion as a neutron dosimeter was evaluated in exposure of a human phantom to neutrons from a plutonium-beryllium source. Emulsion pieces were located at various positions in and around the phantom. The following basic information referring to each location was obtained by scanning 2-cm squares of 600-μ Ilford L.4 emulsion with a semiautomatic three-axis digitized microscope:

1. The relative differential proton-recoil energy spectrum.
2. The absolute differential track-density energy distribution.
3. The average track energy.

From these data, the following dose information may be calculated.

1. The total absolute proton recoil track absorbed dose in tissue.
2. The thermal neutron N(n, p)C dose in tissue.
3. The thermal neutron density and fast neutron flux in tissue.

In addition, the proton recoil spectrum reveals general information about the local fast-neutron energy spectrum.

Acknowledgments

The authors wish to thank Mr. James C. Hodges for the design, construction, and maintenance of the three-axis digitized microscope; Mr. Arthur W. Barnes for the design of the microscope electronics; Mr. John R. Meneghetti for making the phantom; Mr. John H. Wood and Miss Betty J. Lofstrand for processing the L.4 emulsions; Miss Olga M. Fekula for scanning the L.4 emulsions; Miss Dorothy A. Hadley and Miss Josephine A. Camp for scanning the NTA film; Mr. Carl Quong for preparing the computer program; and Mr. H. Wade Patterson and Dr. Roger W. Wallace for their continuous support.

Footnotes and References

*Work done under the auspices of the U.S. Atomic Energy Commission.

1. W.H. Barkas, et al., The Range-Energy Relation in Emulsion, Part II, University of California, Lawrence Radiation Laboratory Report UCRL-3769, April 15, 1957 (unpublished).

2. R.L. Lehman, "Energy Response and Physical Properties of NTA Personnel Neutron Dosimeter Nuclear Track Film," Lawrence Radiation Laboratory Report UCRL-9513, Jan. 13, 1961 (unpublished).

3. Handbook 63, "Protection Against Neutron Radiation up to 30 Million Electron Volts," U.S. Dept. of Commerce, National Bureau of Standards, Nov. 22, 1957.

Table 1. Energy spectrum of proton recoils in emulsions.

Channel	Energy (Mev)	C-1	S. D.	C-2	S. D.	C-3	S. D.	C-4	S. D.	C-5	S. D.	C-9	S. D.
1	0.0												
2	0.030												
3	0.120			16	16	17	17			18	18	17	17
4	0.225	82	41	57	32	103	46	29	20	21	21	40	28
5	0.316	528	112	221	70	384	96	169	53	101	50	284	82
6	0.396	323	93	547	116	377	100	266	71	340	98	424	106
7	0.468	527	124	730	140	469	117	455	97	123	61	375	104
8	0.536	726	151	1341	197	1233	197	915	143	832	166	591	135
9	0.600	535	133	1327	202	1238	203	1395	181	775	165	362	109
10	0.665	768	163	999	179	1188	203	1184	171	552	142	619	145
11	0.723	438	126	876	171	767	167	696	134	577	149	575	143
12	0.805	536	101	442	88	613	108	541	85	585	108	623	108
13	0.897	604	110	409	87	403	90	413	76	488	101	476	97
14	0.998	487	101	313	78	254	73	314	68	355	86	438	95
15	1.092	379	91	226	68	312	83	299	68	517	110	571	112
16	1.183	420	99	366	88	257	77	264	66	541	115	437	100
17	1.282	487	109	225	71	97	48	362	79	411	102	504	110
18	1.364	481	110	163	61	329	91	268	69	453	110	349	93
19	1.443	475	111	268	80	211	74	279	72	194	73	234	78
20	1.521	381	101	125	56	81	47	173	57	430	111	456	110
21	1.597	310	93	78	45	84	48	179	59	267	89	222	78
22	1.688	136	51	144	50	293	75	276	61	308	79	327	79
23	1.792	142	53	206	62	162	57	172	49	256	74	260	72
24	1.911	142	47	175	50	111	41	201	47	300	70	203	56
25	2.040	151	50	139	46	185	55	83	31	88	39	265	66
26	2.180	113	39	117	39	84	34	130	36	193	53	167	48
27	2.320	161	48	81	33	29	20	155	40	185	53	158	47
28	2.490	95	31	49	22	64	26	97	27	168	43	126	36
29	2.700	91	30	37	18	71	26	64	21	85	30	170	41
30	2.900	65	26	101	31	54	24	54	20	103	34	129	37
31	3.100	79	30	63	25	79	30	80	25	144	41	78	29
32	3.30	62	25	38	19	83	29	73	23	77	29	92	30
33	3.50	32	18			21	15	53	20	80	30	42	21
34	3.70	58	26			11	11	49	20	86	32	80	30
35	3.90	44	22	10	10	77	29	46	19	11	11	32	18
36	4.10	46	23	10	10	11	11	40	18	60	27	45	22
37	4.29	10	10	9	9	21	15	7	7	22	15	21	14
38	4.50			10	10	33	19	39	17	46	23	32	18
39	4.70	11	11					42	18	25	17	11	11
40	4.90	11	11					23	13	23	16	21	15
41	5.10	34	19			11	11	8	8	12	12	33	19
42	5.30			11	11			15	11	12	12	21	15
43	5.50									26	18	12	12
44	5.70			11	11	12	12	9	9	13	13		
45	5.90			11	11	12	12					12	12
46	6.10	12	12	11	11					13	13		
47	6.30					12	12	25	15				
48	6.50									26	18	12	12
49	6.80												
50	7.20												
51	7.60												
52	8.00					6	6			7	7		
53	8.40									7	7		
54	8.80			6	6	7	7						
55	9.20					7	7						
56	9.60			7	7			11	7				

Table 2. Cross sections in emulsion and tissue

Element	Atomic density $(\times 10^{22}\ cm^{-3})$	σ_{abs}^{th} $(\times 10^{-24}\ cm^2)$	$\sigma_{total}^{1\ Mev}$ $(\times 10^{-24}\ cm^2)$	$\sigma_{total}^{4\ Mev}$ $(\times 10^{-24}\ cm^2)$	$N\sigma_{abs}^{th}$ (cm^{-1})	$N\sigma_{total}^{1\ Mev}$ (cm^{-1})	$N\sigma_{total}^{4\ Mev}$ (cm^{-1})
Emulsion							
Ag	1.01	62.	6.6	4.2	0.626	0.066	0.082
Br	1.00	6.6	5.0	3.9	0.067	.050	.039
H	3.21	0.33	4.4	1.9	0.011	.142	.061
C	1.38	0.0032	2.6	2.0	0.000	.036	.028
O	0.95	0.19	4.0	2.0	.002	.038	.019
N	0.32	1.83	2.0	1.8	.006	.006	.006
I	.0056	6.7	7.0	5.0	.000	.000	.000
					0.710	.340	.195
Tissue							
H	6.00[a]				0.0200	0.264	0.114
C	0.91[a]				0.0000	.024	.018
O	2.45[a]				0.0000	.098	.049
N	0.13[a]				0.0024	.003	.002
					0.022	0.390	0.180

[a] Assuming density of tissue is 1.00

Table 3. Estimation of the n, p track component in Ilford films

	A_i	k	% thermal np tracks	% thermal neutrons present[a]
C-9	29.48	0.418	0	0
C-1	35.92		8.9	39
C-2	48.47		26.9	76
C-3	47.60		25.7	74.5
C-4	43.80		20.3	69
C-5	32.21		3.9	25

[a]Based on d/c ratio in Eq. (3) of 6.5/1.

Table 4. Energy absorbed from proton recoils in L.4 emulsion and in tissue at various depths in the phantom; PuBe neutron source.

Emulsion	Depth in phantom	Track dose: Thermal n, p (Mev cm^{-3} per n cm^{-2}) L.4 Dose	Thermal n, p Tissue Dose	Fast-neutron – proton recoil[a] (Mev cm^{-3} per n cm^{-2}) L.4 Dose	Fast-neutron – proton recoil[a] Tissue Dose	Total proton (Mev cm^{-3} per n cm^{-2}) L.4 Dose	Total proton Tissue Dose
C-9	air	0		76×10^{-3}		76×10^{-3}	
C-1	0 cm	3.2×10^{-3}	1.3×10^{-3}	83	154×10^{-3}	86	155×10^{-3}
C-2	5 cm	7.9	3.2	51	96	59	99
C-3	10 cm	5.2	2.1	40	76	45	78
C-4	15 cm	2.4	0.98	28	53	30	54
C-5	20 cm	0.20	0.08	15	28	15	28

[a]Normalized to 50 cm by inverse square; also normalized to unit neutron exposure.

Table 5. Comparison of measured tissue proton dose in phantom with Handbook 63 calculated dose for an infinite 30-cm-thick slab of tissue

	Tissue proton dose (rad per $n/cm^2 \times 10^{-9}$)		
Depth	Phantom, PuBe neutrons	HB 63, 2.5-Mev neutrons	HB 63, 5.0-Mev neutrons
0 cm	2.5	3.7	4.8
5 cm	1.6	2.8	4.1
10 cm	1.25	1.4	2.6
15 cm	0.87	0.65	1.7
20 cm	0.45	0.31	1.1

LEGENDS

Fig. 1. Positions of phantom and source.

Fig. 2. Positions of source, phantom, and packets during exposure (as viewed from above).

Fig. 3. Chart used for recording emulsion history.

Fig. 4. Three-axis digitized microscope with supporting electronic equipment.

Fig. 5. Three-axis digitized microscope used in this experiment.

Fig. 6. Energy distribution of recoil protons from PuBe source: Emulsion C-1, at front surface of phantom.

Fig. 7. Energy distribution of recoil protons from PuBe source: Emulsion C-2, 5.65 cm deep in phantom.

Fig. 8. Energy distribution of recoil protons from PuBe source: Emulsion C-3, 10.65 cm deep in phantom.

Fig. 9. Energy distribution of recoil protons from PuBe source: Emulsion C-4, 15.65 cm deep in phantom.

Fig. 10. Energy distribution of recoil protons from PuBe source: Emulsion C-5, 21 cm deep in phantom (on the back surface).

Fig. 11. Energy distribution of recoil protons from PuBe source: Emulsion C-9, 50 cm (in air) from source.

Fig. 12. Track density distributions, at various positions in and around phantom, of recoil protons from neutron irradiation by PuBe source, normalized to 50 cm from source.

Fig. 13. Numbers of tracks in Ilford L.4 emulsion (600μ) at various depths in the phantom.

Fig. 14. Numbers of tracks in Kodak NTA emulsion (30μ) at various depths in the phantom.

Fig. 15. Average energy of recoil protons in nuclear emulsion at various depths in the phantom.

——— experimental data points

– – – data points calculated by omitting thermal n, p tracks

● control in air

Fig. 16. Tissue dose by protons from thermal-neutron-induced N(n, p)C, in phantom exposed to PuBe neutron source.

——— estimated from measurements (this experiment)

– – – thermal-neutron density in phantom, measured by indium foil activation with same exposure conditions (relative numbers only, to allow comparison of curve shapes).

Fig. 17. Proton-recoil energy absorbed per cm^3 of Ilford L. 4 emulsion at various depths in the phantom.

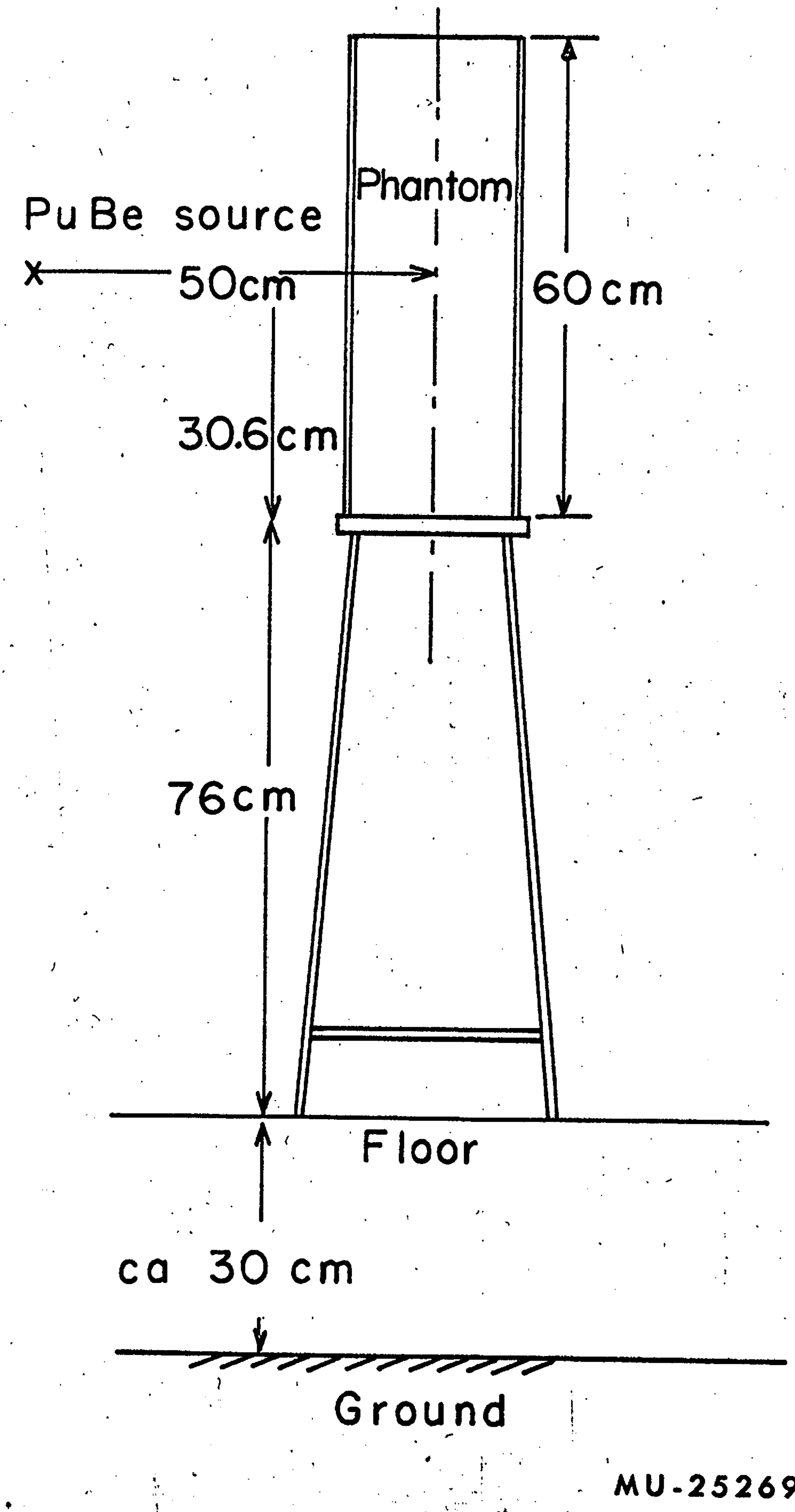
Phantom
PuBe source
50cm
60 cm
30.6 cm
76 cm
Floor
ca 30 cm
Ground
MU-25269

Fig. 1

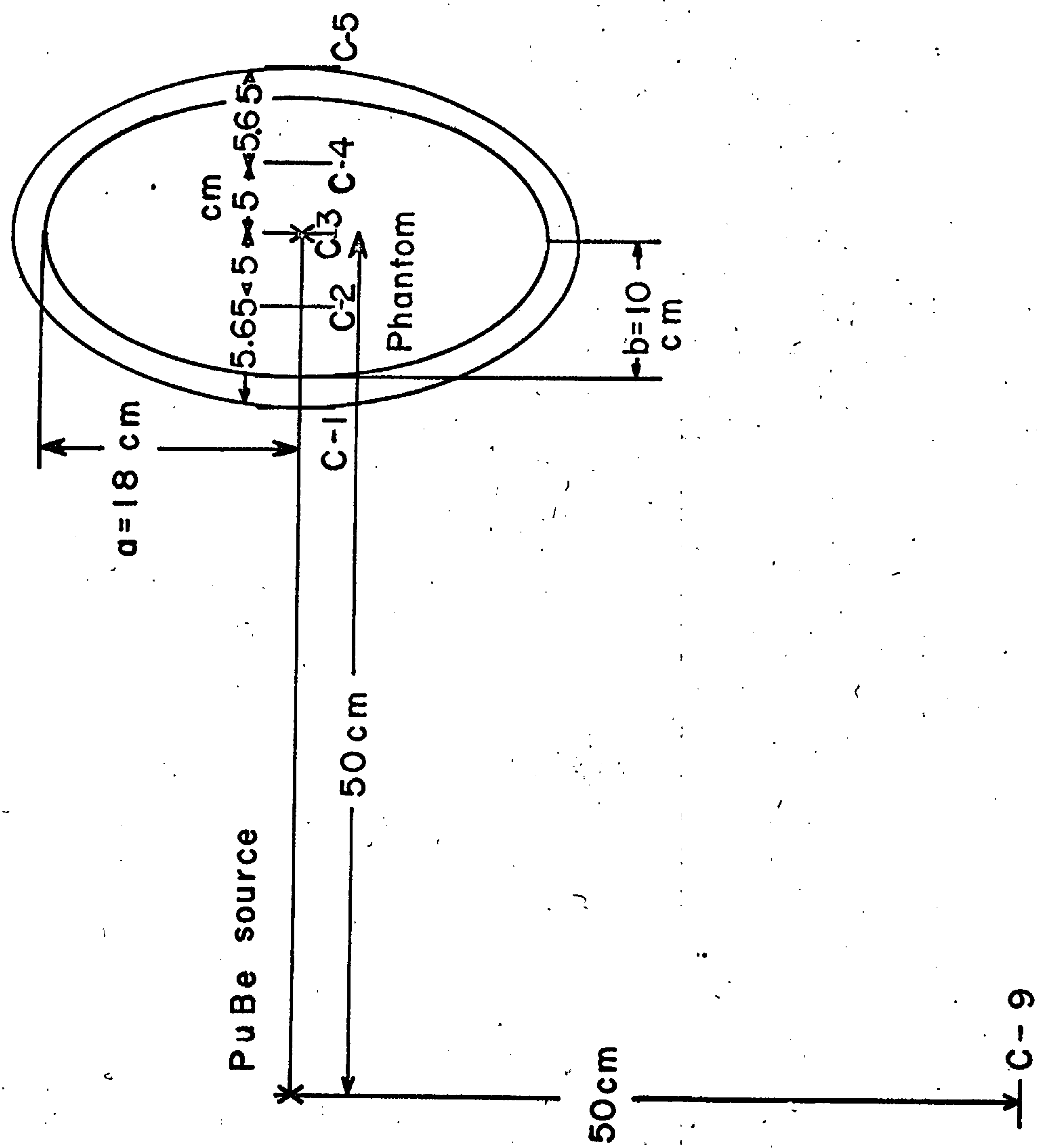

MU-25270

Fig. 2

EMULSION HISTORY CHART

Emulsion # ______ Type ______ Batch code ______
Date Manufactured ______ Date of arrival at UCLRL ______
Storage: Location ______ Dates ______ to ______
Location ______ Dates ______ to ______
Location ______ Dates ______ to ______

Exposure: Location ______ Type of exposure ______
Duration ______ to ______ Distance from source ______
Orientation ______
Scattering conditions ______
Diagram ______

Development: Procedure ______
Personnel ______
Location ______ Dates ______ to ______
Comments ______

Mounting: 1 × 3 glass slide ______ Epoxy cement ______ Date ______ Person ______
Comments ______

Scanning: Scanner ______ No. of tracks ______ Dates ______ to ______
Scanner ______ No. of tracks ______ Dates ______ to ______
Location of data cards ______ Emulsion code no. ______ f_1 ______ f_2 ______
Comments ______

Analysis: Program ______ Tracks used ______ Date ______ Person ______
Program ______ Tracks used ______ Date ______ Person ______
Program ______ Tracks used ______ Date ______ Person ______
Comments ______

Shrinkage: Thickness before presoak - micrometer (inches)
Date ______ RH ______ .02 .02 .02 .02 .02 Av 0.02 in.
Thickness after development - before mounting - micrometer
Date ______ RH ______ .01 .01 .01 .01 .01 Av 0.01 in.
Thickness after mounting - microscope
Date ______ RH ______ Average ______ $\mu \times .393 =$ 0.0 in.

Lateral Distortion: Dimensions before presoak - 64th inch scale
Date ______ /64 /64 /64 /64 Av /64
Dimensions after development - before mounting
Date ______ /64 /64 /64 /64 Av /64
Dimensions after mounting
Date ______ ______ ______ ______ ______ ______

Subsequent Measurements: ______

MU-25249

Fig. 3

Fig. 4

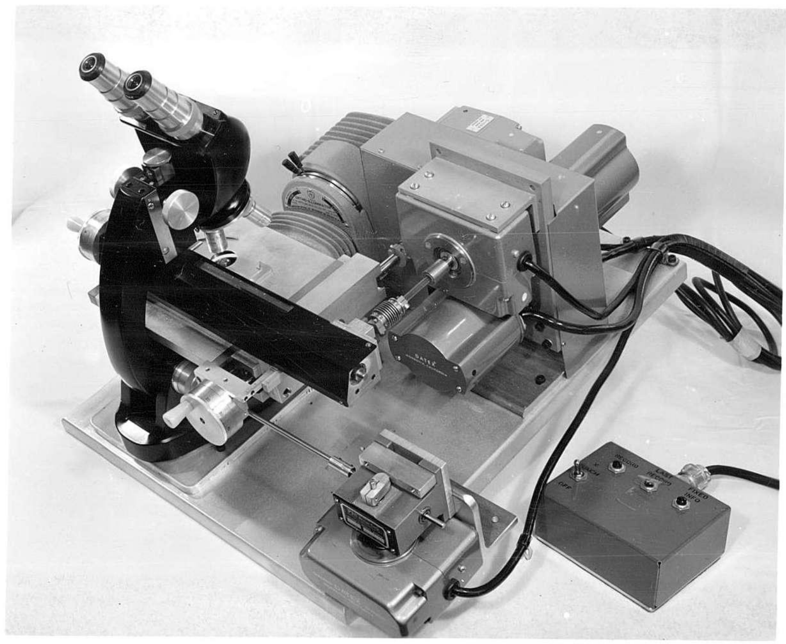

Fig. 5

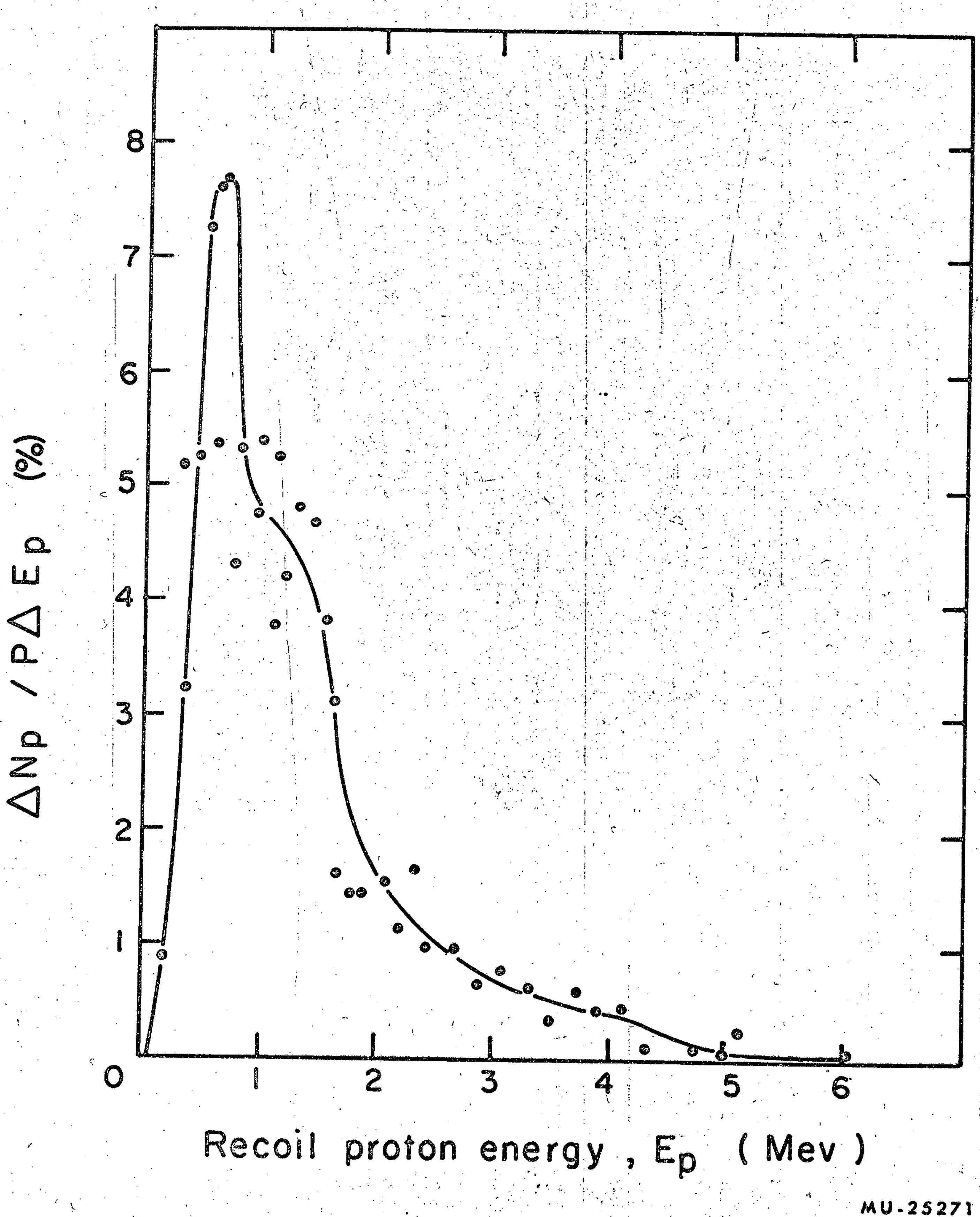

8
7
6
5
4
3
2
1
0
1
2
3
4
5
6
ΔNp / PΔ Ep (%)
Recoil proton energy, Ep (Mev)
MU-25271

Fig. 6

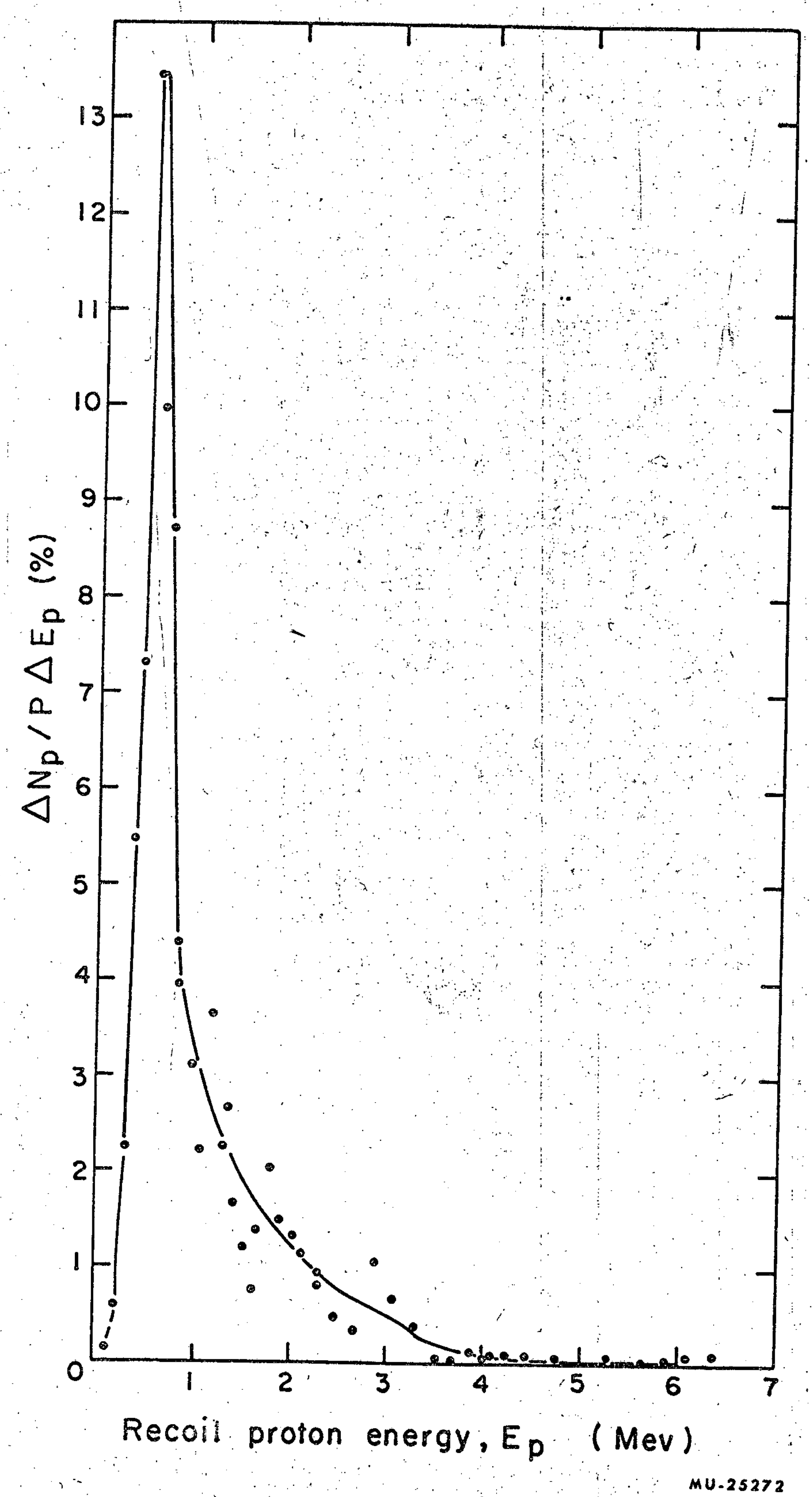

13
12
11
10
9
8
7
6
5
4
3
2
1
0
$\Delta N_p / P \, \Delta E_p$ (%)
0
1
2
3
4
5
6
7
Recoil proton energy, E_p (Mev)
MU-25272

Fig. 7

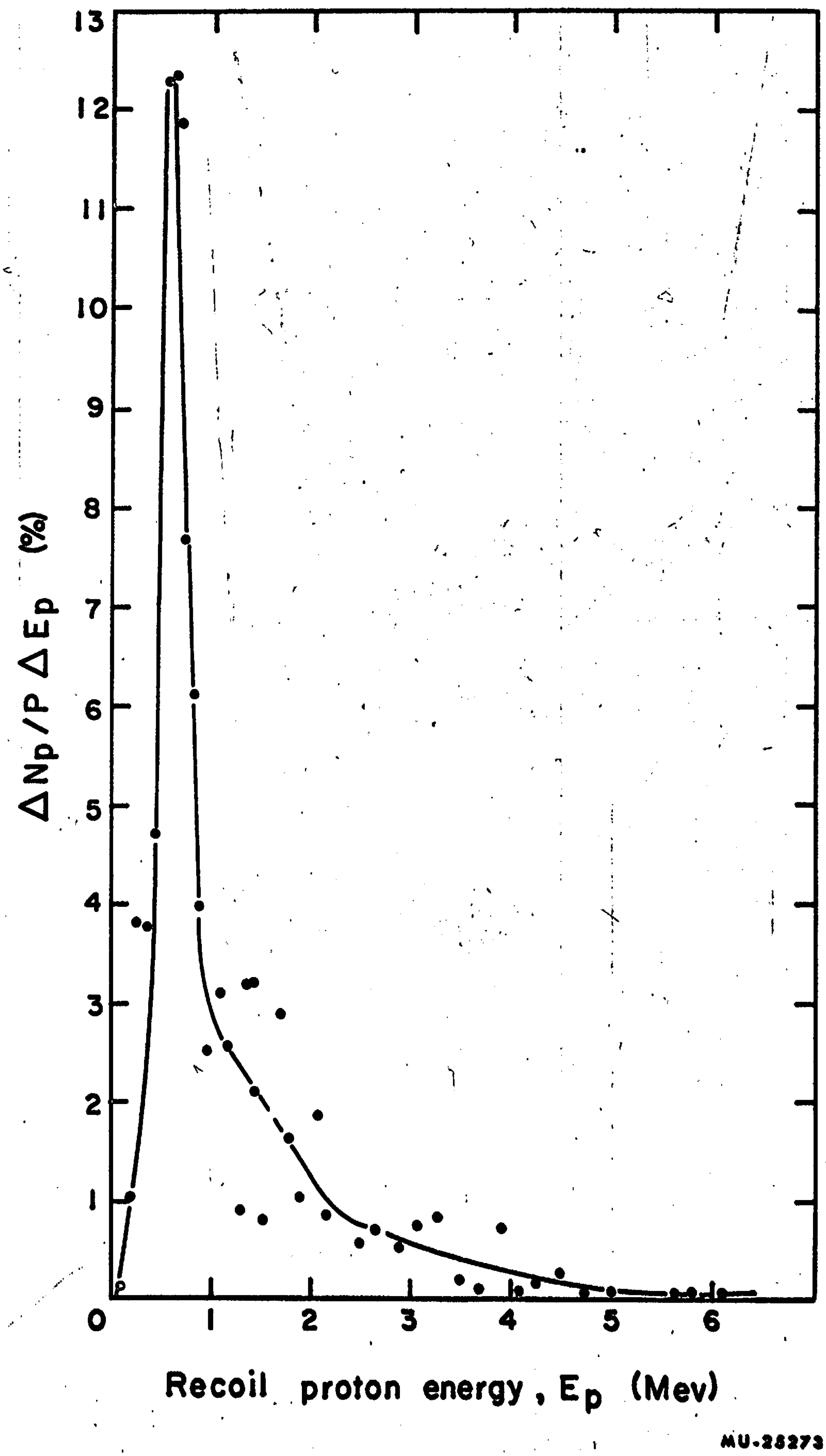
13
12
11
10
9
8
7
6
5
4
3
2
1
0
1
2
3
4
5
6
ΔNp/P ΔEp (%)
Recoil proton energy, Ep (Mev)
MU-25273

Fig. 8

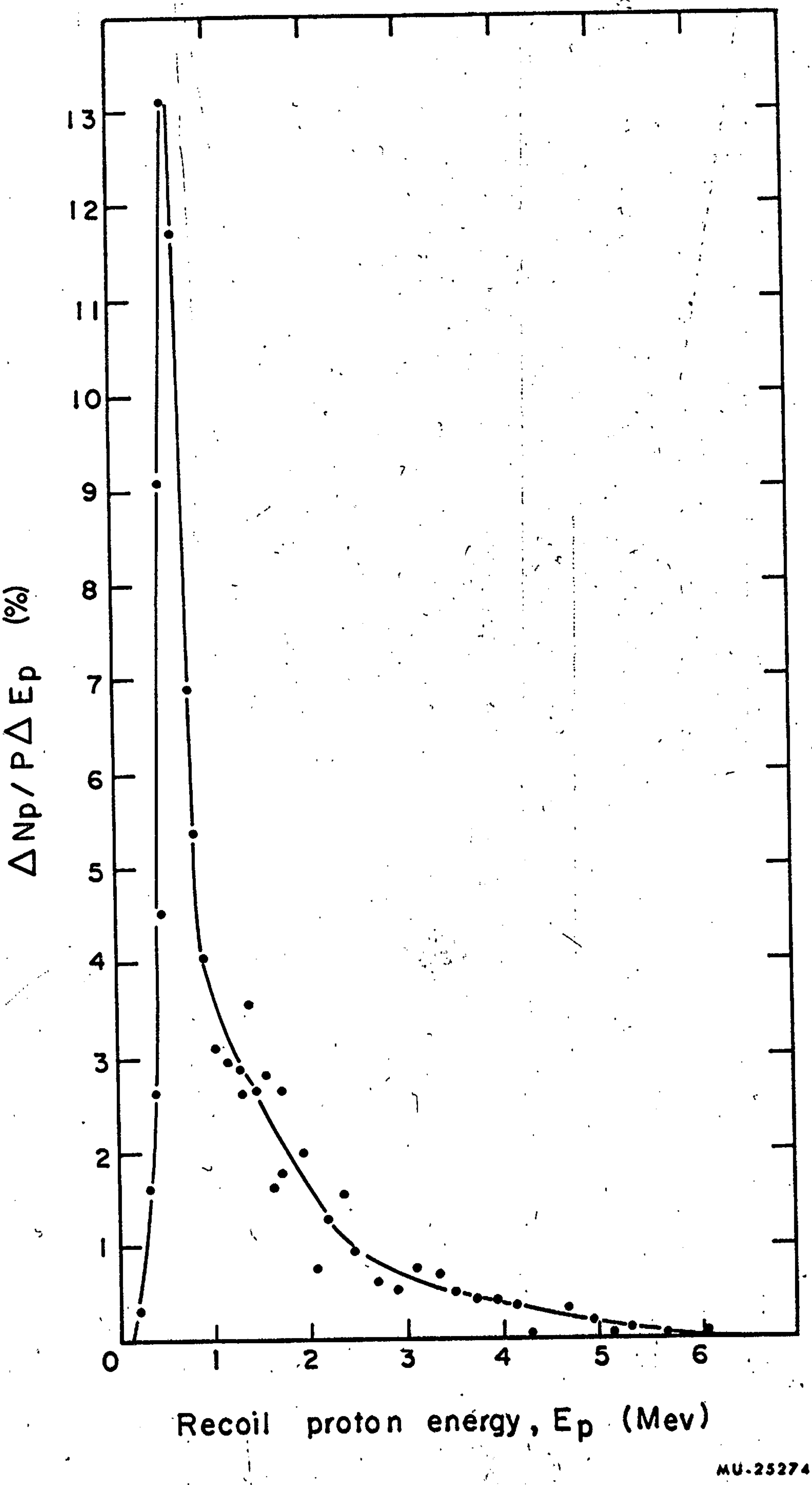
13
12
11
10
9
8
7
6
5
4
3
2
1
0
1
2
3
4
5
6
ΔNp / P Δ Ep (%)
Recoil proton energy, Ep (Mev)
MU-25274

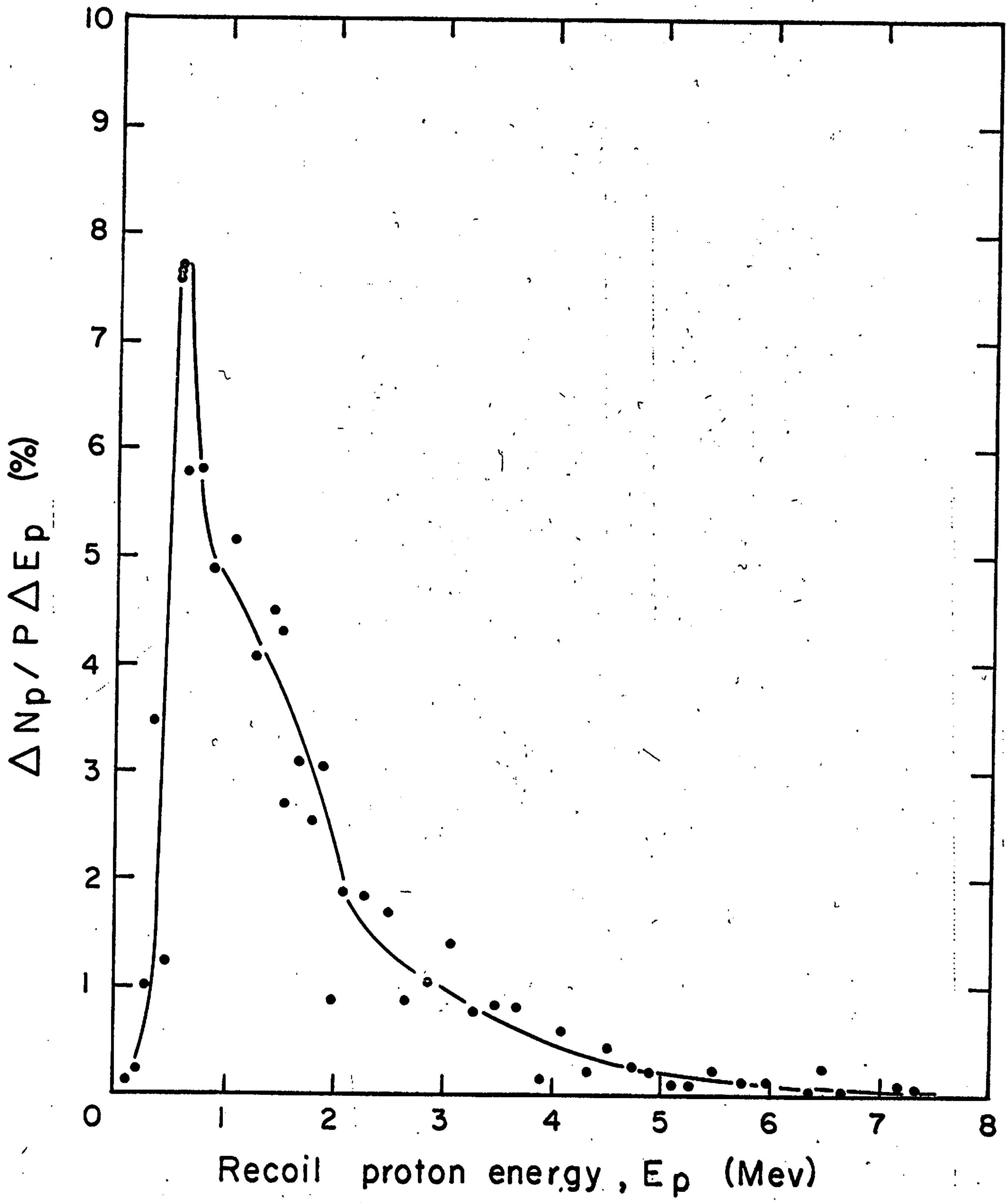
10
9
8
7
6
5
4
3
2
1
0
ΔNp/PΔEp (%)
1
2
3
4
5
6
7
8
Recoil proton energy, Ep (Mev)

MU-25275

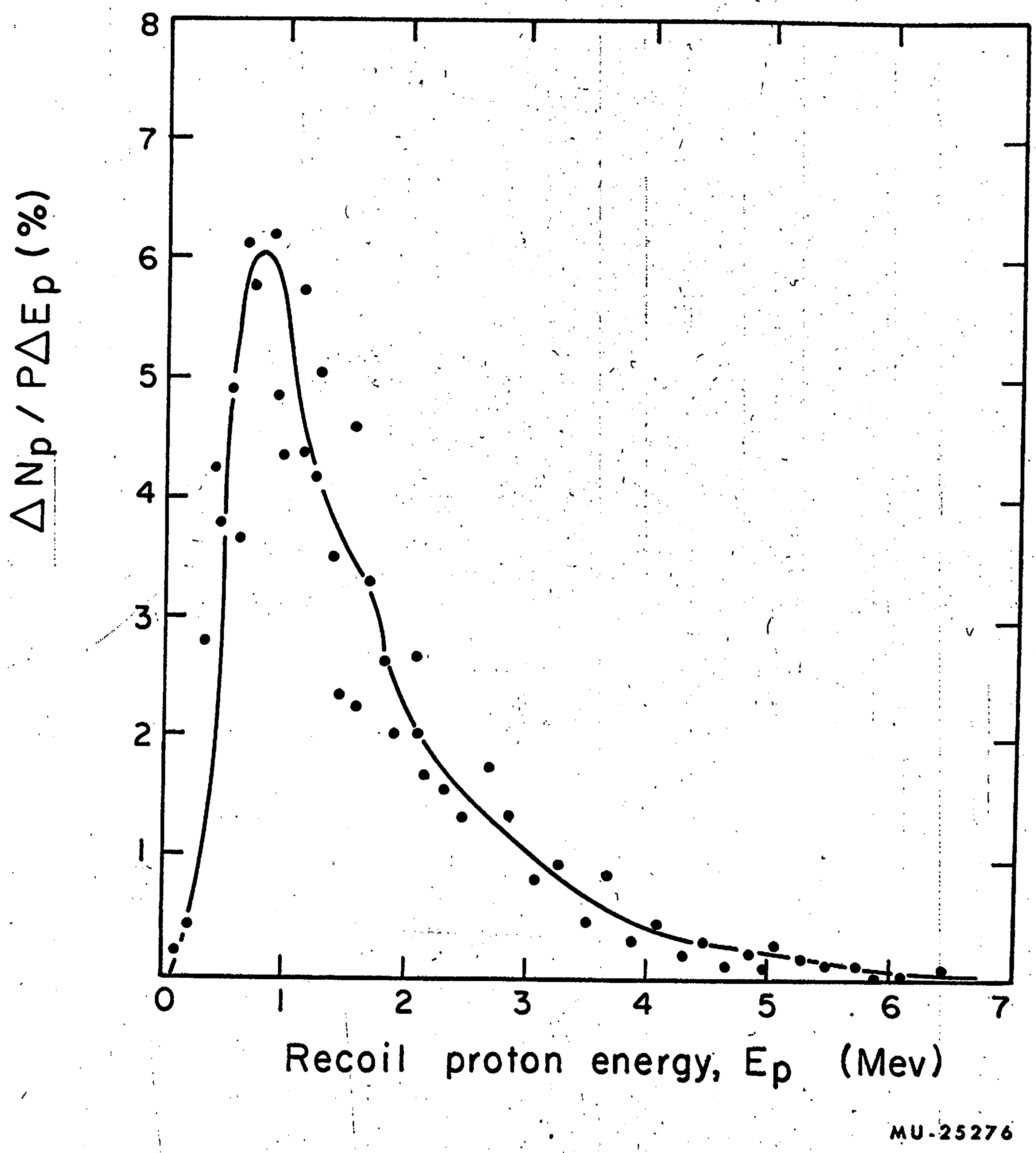
8
7
6
5
4
3
2
1
0
1
2
3
4
5
6
7
ΔNp / PΔEp (%)
Recoil proton energy, Ep (Mev)
MU-25276

Fig. 11

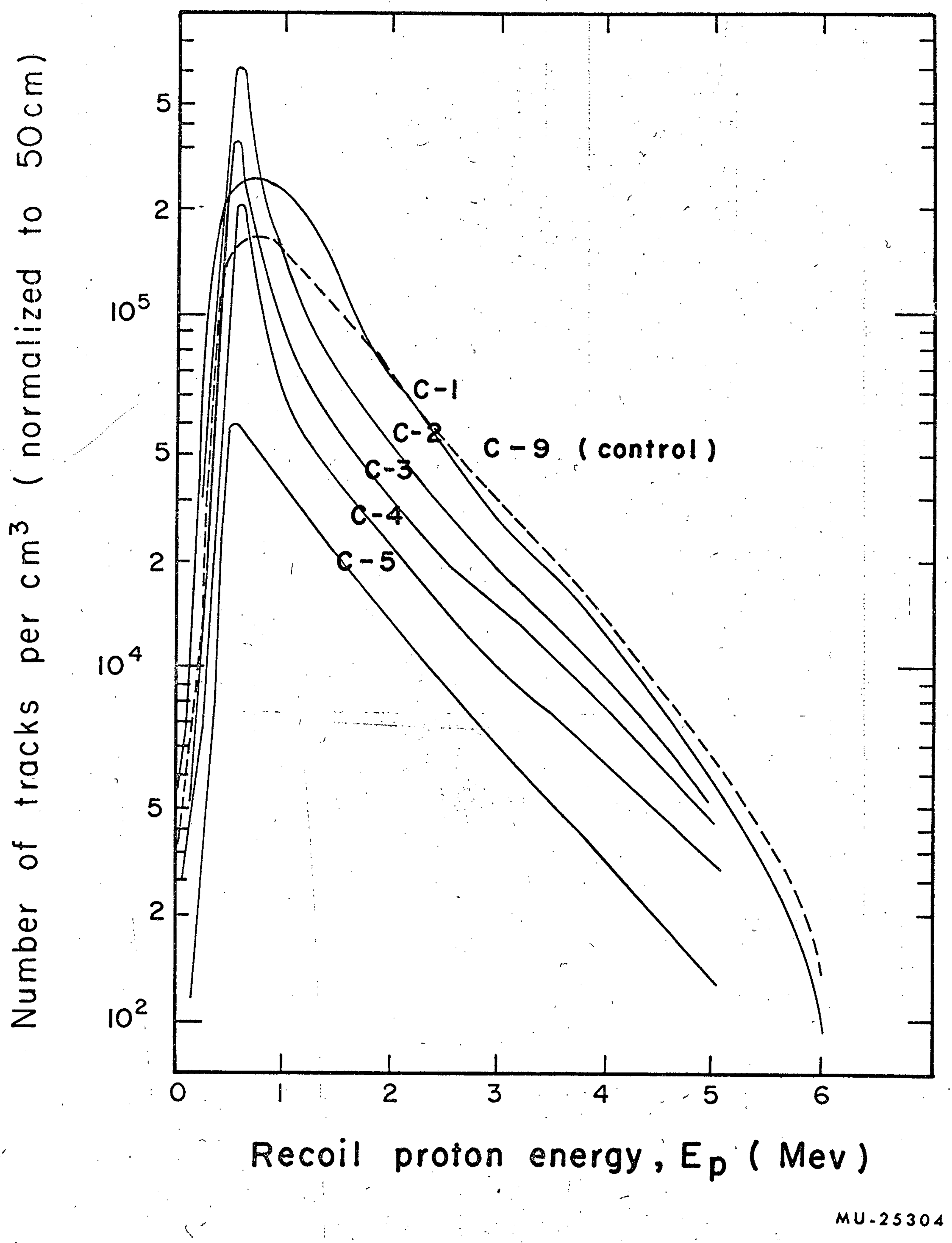
Number of tracks per cm^3 (normalized to 50cm)
Recoil proton energy, E_p (Mev)
5
2
10^5
5
2
10^4
5
2
10^2
0
1
2
3
4
5
6
C-1
C-2
C-9 (control)
C-3
C-4
C-5
MU-25304

Fig. 12

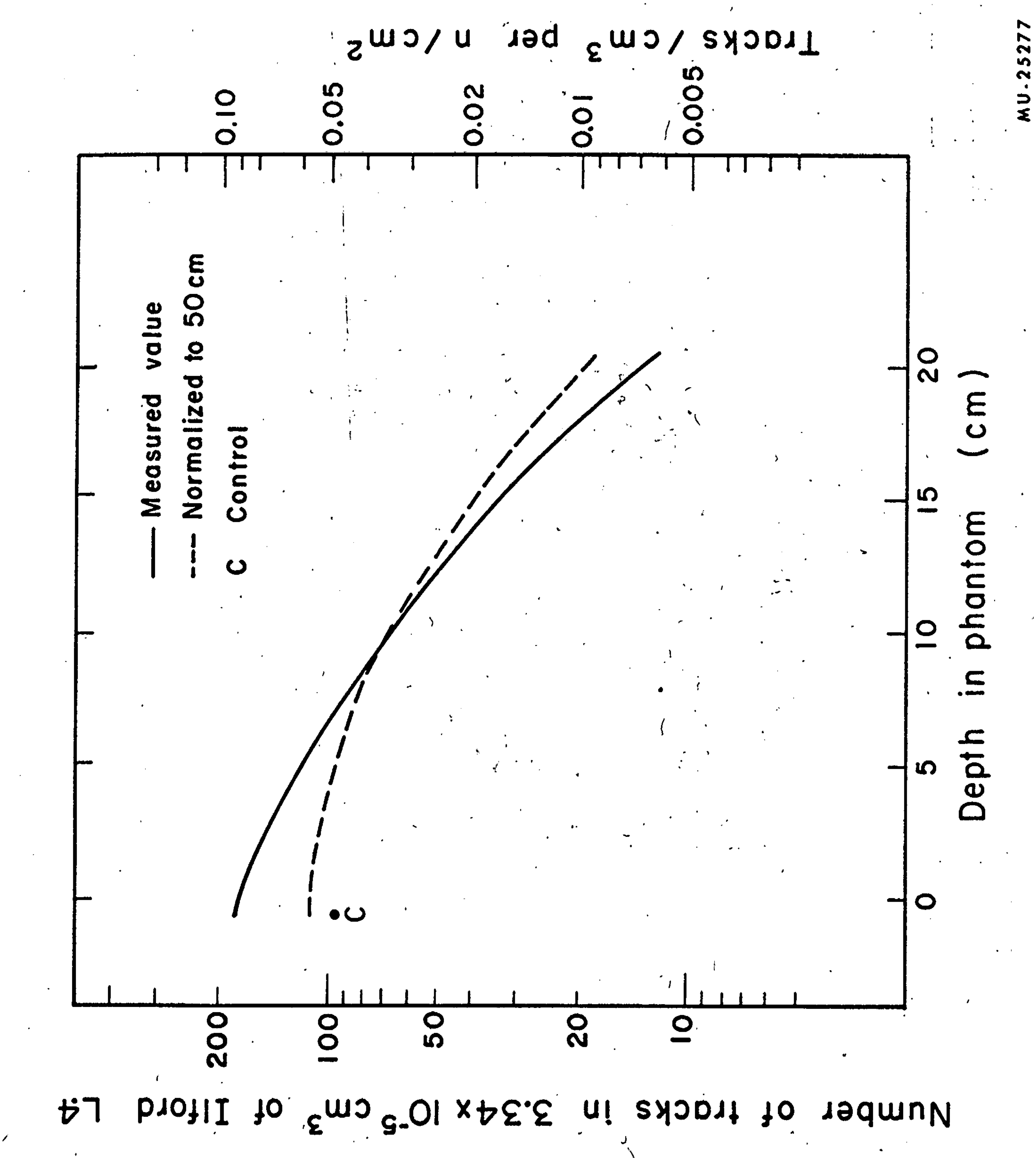
Tracks / cm³ per n / cm²
0.10
0.05
0.02
0.01
0.005
Measured value
Normalized to 50 cm
C Control
C
Number of tracks in 3.34x10⁻⁵ cm³ of Ilford L4
200
100
50
20
10
0
5
10
15
20
Depth in phantom (cm)
MU-25277

Fig. 13

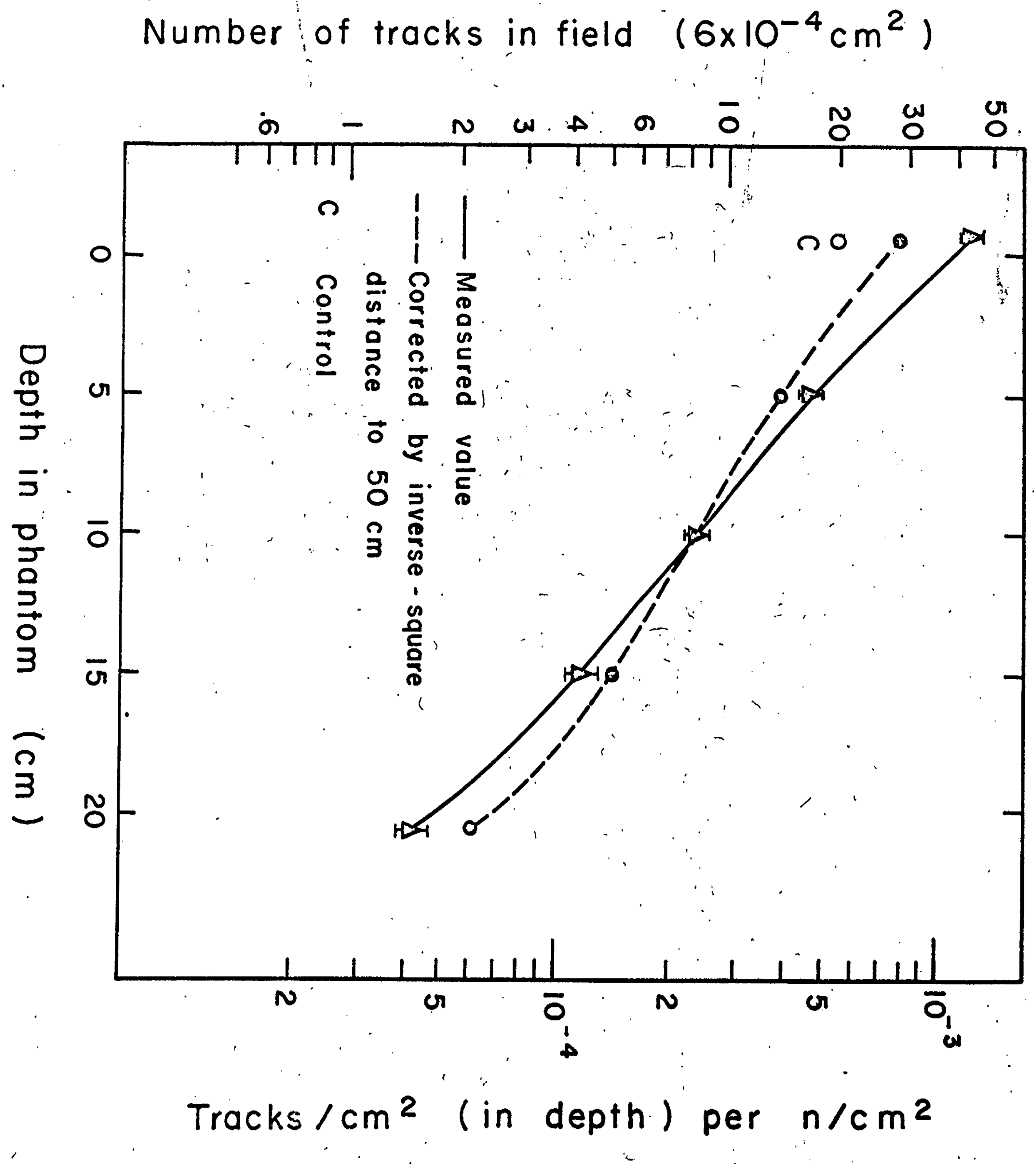
Number of tracks in field $(6 \times 10^{-4} cm^2)$
.6
1
2
3
4
6
10
20
30
50
Measured value
Corrected by inverse-square distance to 50 cm
C Control
o
C
0
5
10
15
20
Depth in phantom (cm)
2
5
10^{-4}
2
5
10^{-3}
Tracks / cm^2 (in depth) per n/cm^2
MU-25278

Fig. 14

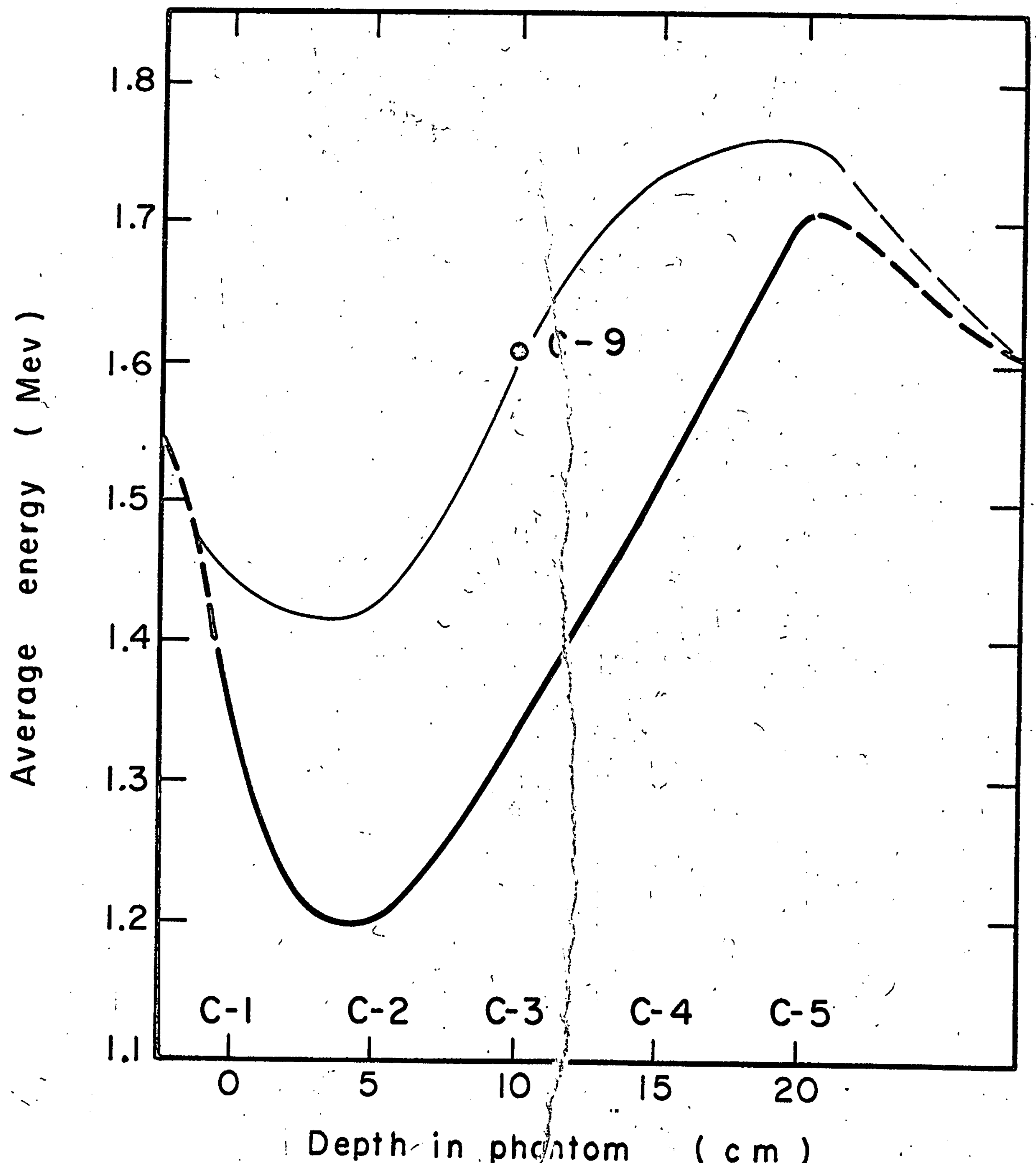

MU-25279

Fig. 15

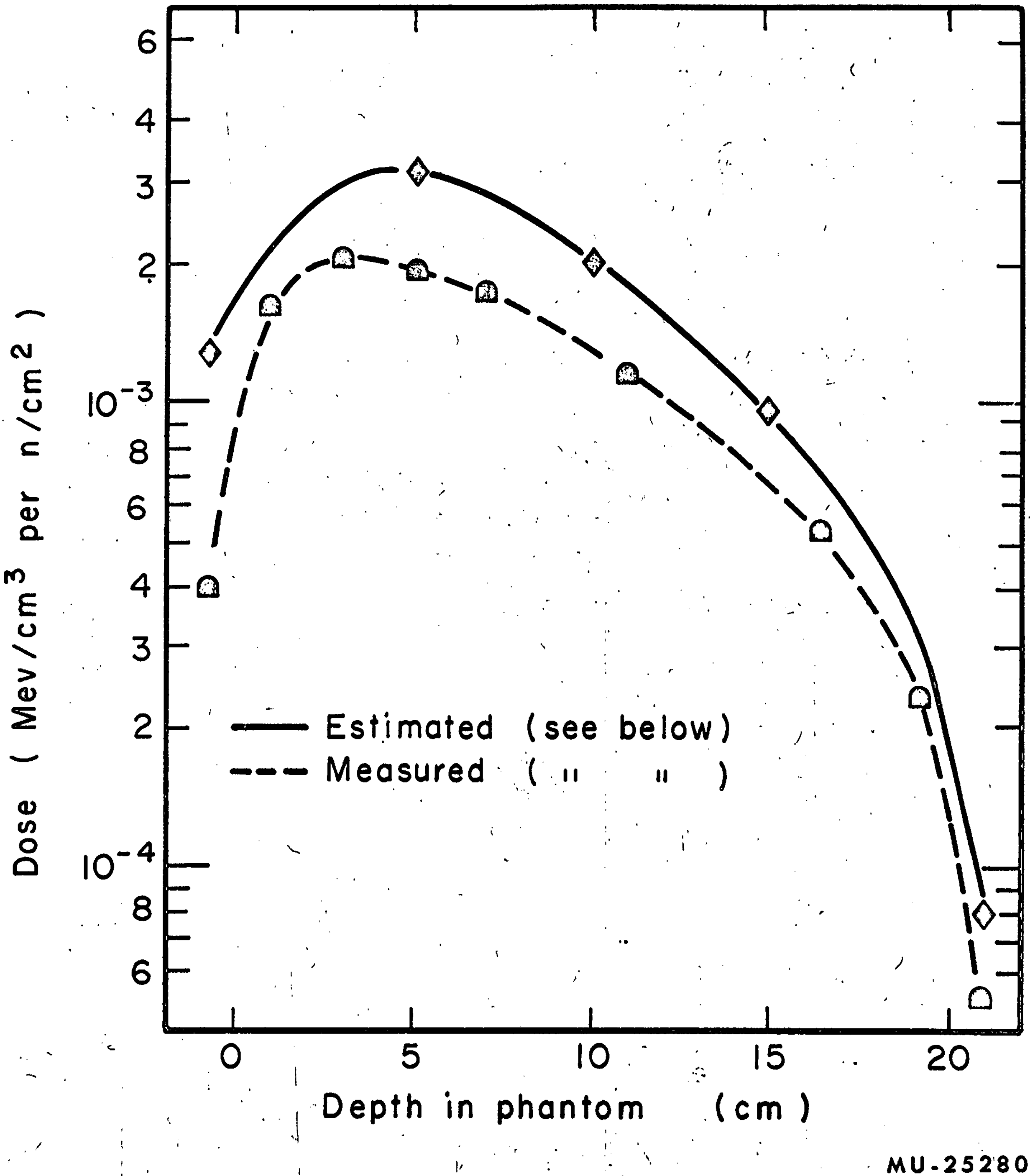
6
4
3
2
10^{-3}
8
6
4
3
2
10^{-4}
8
6
0
5
10
15
20
Dose (Mev/cm^3 per n/cm^2)
Depth in phantom (cm)
Estimated (see below)
Measured (" ")
MU-25280

Fig. 16

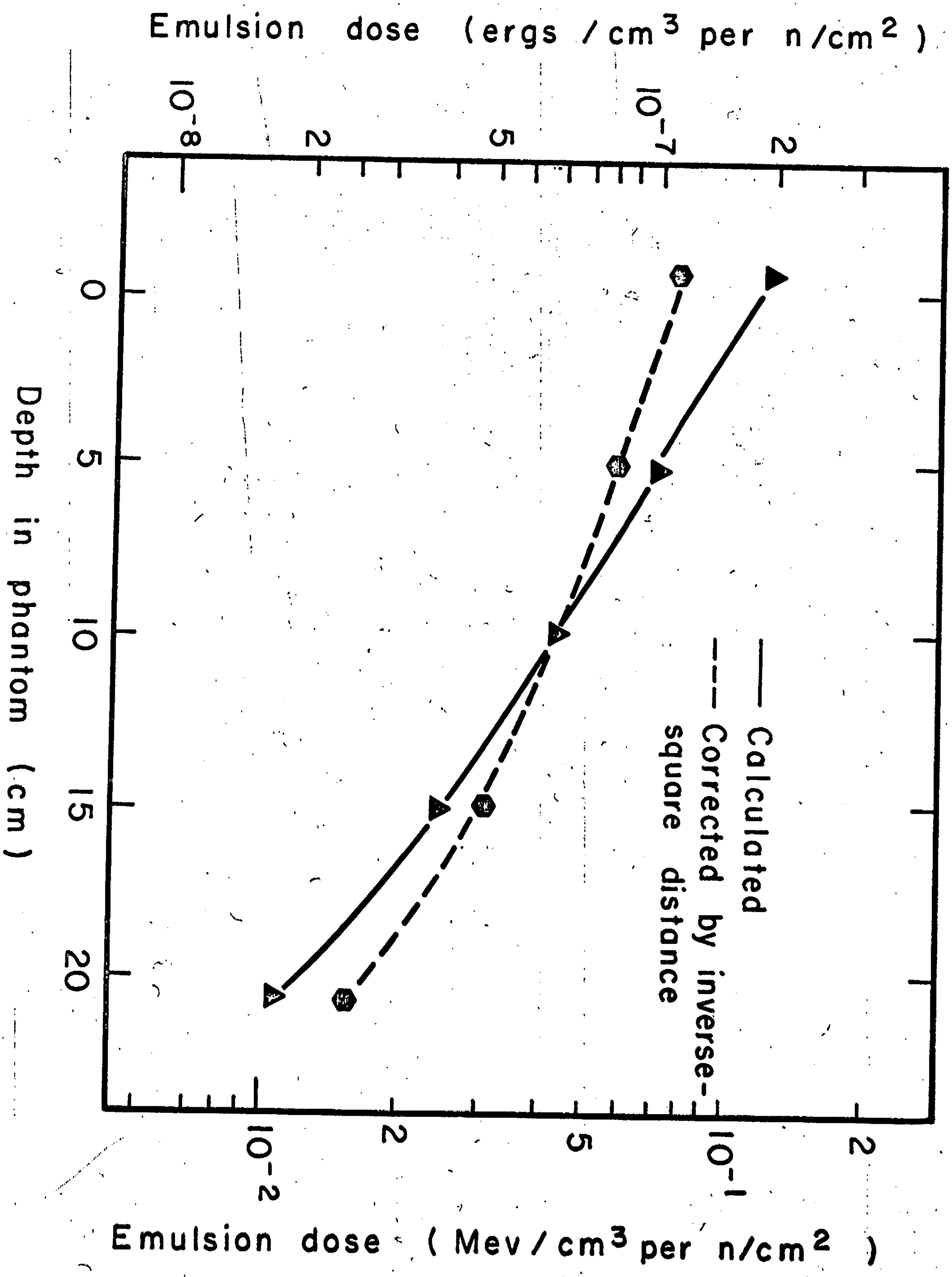

MU-25281

Fig. 17